Transmural Contractile Reserve After Reperfused Myocardial Infarction in Dogs

Jérôme Garot, MD,* David A. Bluemke, MD, PHD,† Nael F. Osman, PHD,‡ Carlos E. Rochitte, MD,*
Elias A. Zerhouni, MD,† Jerry L. Prince, PHD,‡ João A.C. Lima, MD, FACC*

Baltimore, Maryland

OBJECTIVES	The goal of this study was to characterize detailed transmural left ventricular (LV) function at rest and during dobutamine stimulation in subendocardial and transmural experimental infarcts.
BACKGROUND	The relation between segmental LV function and the transmural extent of myocardial necrosis is complex. However, its detailed understanding is crucial for the diagnosis of myocardial viability as assessed by inotropic stimulation.
METHODS	Short-axis tagged magnetic resonance images were acquired at five to seven levels encompassing the LV from base to apex in seven dogs 2 days after a 90-min closed-chest left anterior descending coronary occlusion, followed by reflow. Myocardial strains were measured transmurally in the entire LV by harmonic phase imaging at rest and 5 ig.kg^{-1}.min^{-1} dobutamine. Risk regions were assessed by radioactive microspheres, and the transmural extent of the infarct was assessed by 2,3,5 triphenyltetrazolium chloride staining.
RESULTS	Circumferential shortening (Ecc), radial thickening (Err) and maximal shortening at rest were greater in segments with subendocardial versus transmural infarcts, both in subepicardium (-1.1 ± 1.0 vs. $2.5 \pm 0.6\%$ for Ecc, -0.5 ± 1.9 vs. $-1.8 \pm 1.0\%$ for Err, $p < 0.05$) and subendocardium (-2.0 ± 1.4 vs. $2.8 \pm 0.8\%$, 2.4 ± 1.7 vs. $0.0 \pm 0.9\%$, respectively, $p < 0.05$). Under inotropic stimulation, risk regions retained maximal contractile reserve. Recruitable deformation was found in outer layers of subendocardial infarcts ($p < 0.01$ for Ecc and Err) but also in inner layers ($p < 0.01$). Conversely, no contractile reserve was observed in segments with transmural infarcts.
CONCLUSIONS	Under dobutamine challenge, recruitment of myofiber shortening and thickening was observed in inner layers of segments with subendocardial infarcts. These results may have important clinical implications for the detection of myocardial viability. (J Am Coll Cardiol 2000;36:2339–46) © 2000 by the American College of Cardiology

The accurate assessment of myocardial viability is an important clinical issue for patients with myocardial infarction (MI) and for those with chronic ischemic left ventricular (LV) dysfunction (1). The evaluation of myocardial contractile reserve by dobutamine stimulation represents a widely used technique for the detection of local viability after MI (1–3). Although crucial to clinical decision making, the recruitment of regional LV function, using echocardiography or magnetic resonance imaging (MRI) is currently based on the qualitative visual analysis of endocardial excursion or myocardial wall thickening (3,4). However, because of the complex fiber orientation in the normal human heart (5) and close interactions between fibers, small amounts of myofiber shortening across the LV wall may lead to passive subendocardial wall thickening (6). Studies by Holmes et al. (7) using implantable beads and by Rademakers et al. (8) using MR myocardial tagging have

demonstrated that the utilization of systolic myocardial wall thickening alone to assess postinfarction local cardiac performance is not always adequate. However, the relationship between recruited segmental LV function during dobutamine stimulation and the transmural extent of myocardial necrosis is largely unknown. This is of great importance given that clinical decision making regarding myocardial viability is in large part based on the measurement of segmental function at rest and during catecholamine stimulation.

Harmonic phase (HARP) MRI (9–14) is a novel technique that provides fast quantitative analysis of regional myocardial strains from tagged cardiac images. Strains can be assessed in a fast and automated way, making the on-line quantitation of regional cardiac function feasible during stress testing in humans. Its sensitivity to detect small alterations of myocardial strain fields during inotropic stimulation has been demonstrated (14). To determine the relation of recruitable local myocardial deformation to transmural myocardial viability, a detailed analysis of the transmural distribution of various regional myocardial strains was performed using HARP from tagged images of reperfused experimental infarcts. Strains obtained at rest and during inotropic stimulation were correlated with histopathologic specimens and regional myocardial blood flow (MBF). The results may have important implications to the

Abbreviations and Acronyms	
Ecc	= circumferential shortening
ECG	= electrocardiogram
Err	= radial thickening
E_1	= maximal elongation
E_2	= maximal shortening
HARP	= harmonic phase imaging
LV	= left ventricular
MBF	= myocardial blood flow
MI	= myocardial infarction
MRI	= magnetic resonance imaging
TTC	= 2,3,5 triphenyltetrazolium chloride

noninvasive assessment of myocardial viability for patients with acute MI.

METHODS

Animal studies are in compliance with animal welfare regulations of the authors' institution and the Food and Drug Administration guidelines and conform to the position of the American Heart Association on research animal use.

Experimental preparation. Seven mongrel dogs weighing 20 to 25 kg were anesthetized with sodium pentobarbital (25 mg·kg^{-1} intravenously), intubated and connected to a respirator. A 6F pigtail catheter was introduced via the right femoral artery into the left ventricle and was used for microsphere administration and LV pressure monitoring. The sheath of this catheter was used for microsphere reference sampling from the femoral artery. A 7F sheath was placed in the left femoral artery, and a 7F left Judkins 2.5 guiding catheter was introduced into the left main coronary artery. An angioplasty balloon catheter was slid into the left anterior descending coronary artery. The balloon was inflated 90 min at 8 atm in the midportion of the left anterior descending coronary artery and then deflated. The AvL lead of the electrocardiogram (ECG) was continuously monitored. Regional MBF was measured immediately before coronary occlusion, 80 min after occlusion and again at 48 h (rest and dobutamine), by LV injection of approximately 2 million sonicated microspheres labeled with either ^{153}Gd, ^{113}Sn, ^{103}Ku, ^{95}Nb or ^{46}Sc.

MRI protocol. Forty-eight hours after reflow, the animals were anesthetized and ventilated. Images were acquired during multiple breath-holds on a 1.5 T whole body magnet (Signa, General Electric Medical Systems, Milwaukee, Wisconsin). Animals were placed in the right anticubital position with electrodes for ECG gating, and a flexible phased-array coil was wrapped around the chest for signal acquisition. The imaging protocol was based on an ECG-triggered segmented k-space fast-gradient echocardiography imaging pulse sequence (15). The tagging pulse sequence consisted of nonselective radiofrequency pulses separated by spatial modulation of magnetization encoding gradients to achieve tag separation of 7 mm.

Contiguous stacks of five to seven base-to-apex short-axis cross-sections were prescribed to encompass the entire LV from base to apex. Two sets of identical short-axis views were acquired (the second set rotated by 90°). This imaging sequence with partial k-space filling and fractional echocardiography to reduce echo time allowed us to image five slices within five breath-holds (approximately 14 s each). Reproducible diaphragmatic positions were obtained by stopping the respirator at end expiratory volume. After rest acquisitions dobutamine was intravenously administered at 5 μg·kg^{-1}·min^{-1} starting 5 min before stress imaging, with continuous blood pressure and ECG monitoring. The acquisition of five to seven short-axis slices took approximately 3 to 4 min, and dobutamine infusion was then stopped. Scanner settings were field of view 32 cm, tag separation 7 mm, 8 mm slice thickness, repetition time 6.5 ms, TE 2.3 ms, 15° tip angle, 256 × 160 image matrix, five to seven views per cine-sequence.

Infarcted, risk and remote regions. After imaging, the heart was arrested with intravenous potassium chloride and excised. The LV was sectioned from base to apex into five to seven equally distant short-axis slices. The junction between the right ventricular free wall and the LV inferior septum was identified on each slice and used as the landmark for later registration with corresponding MR images. The myocardial slices were incubated in a 2% solution of 2,3,5 triphenyltetrazolium chloride (TTC). Regions that failed to demonstrate brick red staining were considered to represent infarcted myocardium (16). For each slice a shallow cut was made to divide the LV circumference into 12 pie-shaped sections. Each section was further subdivided into three to five pieces of approximately equal thickness from the endocardial to the epicardial border. The exact locations of these cuts were recorded before the slices were photographed to relate TTC regions to the location from which tissue samples were taken for microsphere blood flow counting. Each myocardial sample was weighted and counted in a gamma-emission spectrometer along with the reference blood samples. Regional MBF (ml·min^{-1}·g^{-1}) was calculated by standard methods (17). On the basis of TTC staining and microsphere counting, each sample was classified as infarcted (failure to stain by TTC), risk (brick red by TTC with MBF reduced by ≥50% during the occlusion vs. remote) and remote regions (brick red by TTC with unaltered MBF during coronary occlusion). Infarcted regions were further divided into segments with subendocardial (one-third of wall thickness) or transmural infarcts (>one-third of wall thickness).

Strain analysis. The technical aspects of HARP have been described in detail elsewhere (12–14). Harmonic phase imaging is based on the use of isolated peaks in the Fourier domain extracted with a bandpass filter. The inverse Fourier transform of one of these peaks is a complex image whose phase is linearly related to a directional component of the true motion. The slopes of phases reflect the frequency of the tag pattern, and phase images reflect motion of the heart
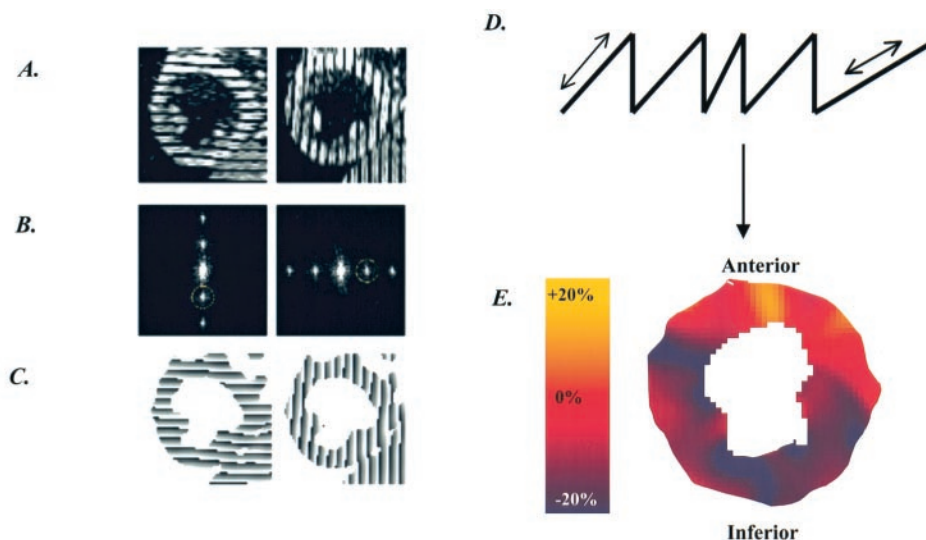
Figure 1. Tagged images of the left ventricular short-axis view (**A**), the magnitudes of the corresponding Fourier transform (**B**) and the corresponding phase images (**C**) in a dog with anterior infarct. The **circles** in the Fourier domain correspond to the size of the bandpass filter. Myocardial strain is directly related to the derivative of the phase, that is, the slope of the phase pattern (**D**). (**E**) Shows the left ventricular map of circumferential strain obtained by harmonic phase imaging in the same animal. **Black** indicates shortening, whereas **yellow** indicates stretching.

(Fig. 1). Tagged-image data sets consisted of 100 to 196 images (five to seven slices, five to seven phases, two directions, rest and dobutamine). Two-dimensional myocardial strains were assessed off-line in 12 pie-shaped myocardial segments. In-plane registration was achieved by matching the coordinates of the posterior junction between the right and LV of the short-axis myocardial strain images to the TTC and MBF maps. Eulerian strains were calculated using single-shot HARP, as previously described (12). Transmural strains were assessed between the reference (end-diastole) and the deformed state (end-systole) as fractional changes in length in the circumferential (E_{cc}) and radial directions (E_{rr}) in the subendocardial, midwall and subepicardial layers. A negative value stands for compression of a line segment between two material points (shortening or thinning), while positive values reflect strain elongation (stretching or thickening) depending on the direction of deformation (circumferential or radial, respectively). In addition, we calculated maximal shortening (E_2) and maximal elongation (E_1) as principal strains given by the magnitude as well as the directions of the associated eigenvectors (14). Since E_1 and E_2 directions are perpendicular, the direction of E_1 was not included in the data.

Statistical analysis. Mean values were expressed as mean ± SEM. Analysis of variance was used for comparisons of myocardial strains and MBF measurements between regions and over time. We used repeated-measures analysis

of variance and the post hoc Tukey's correction for multiple comparisons. All tests were two-tailed, and a p value <0.05 was considered statistically significant.

RESULTS

MBF. Absolute MBF measurements are shown at different time points during the experimental protocol in Table 1. During total coronary occlusion and 48 h later, MBF was lower in infarcted regions as compared with remote regions (p < 0.01). At 48 h MBF was not significantly different in risk regions versus remote regions. In all regions dobutamine stimulation resulted in a significant increase in local myocardial perfusion (p < 0.01), which was less intense in infarcted versus remote regions (p < 0.01). There was no statistical difference in MBF between risk and remote regions.

Strains at rest. *Infarcted, risk and remote regions.* Of the 504 segments analyzed, 314 were categorized as TTC positive and 190 as TTC negative. The extent of MI measured by TTC averaged 25.9 ± 6.1% (range 9 to 50%) of LV surface area. Among the 314 TTC positive segments, 75 were categorized as within the risk region, i.e., underperfused by radioactive microspheres during coronary occlusion. Circumferential shortening, E_{rr} as well as principal strains (E_1, E_2) decreased transmurally in the risk and infarcted regions relative to the remote region (p < 0.0001) (Table 2).

Table 1. Absolute Myocardial Blood Flow

MBF (ml·min^{-1}·g^{-1})	Baseline	Occlusion	Rest 48 h	Dobutamine 48 h
Remote	1.15 ± 0.12	0.97 ± 0.07	1.10 ± 0.11	2.05 ± 0.47†
Risk	1.18 ± 0.14	0.29 ± 0.05*	1.02 ± 0.10	1.83 ± 0.33†
Infarcted	1.16 ± 0.12	0.08 ± 0.02*	0.70 ± 0.09*	1.10 ± 0.23*†

MBF = absolute regional myocardial blood flow. *p < 0.01 vs. remote; †p < 0.01 vs. rest.

Table 2. Myocardial Strains in Remote, Risk and Infarcted Regions

Myocardial Strain (%)	Remote (n = 239)	Risk (n = 75)	TTC Negative Infarcted Regions	
			≤1/3 Wall (n = 61)	>1/3 Wall (n = 129)
E_{cc}				
Endo	−14.7 ± 0.4	−2.5 ± 0.7*	−2.0 ± 1.4*	2.8 ± 0.8*‖‡
Mid	−11.6 ± 0.4	−2.2 ± 0.6*	−1.4 ± 1.1*	2.7 ± 0.6*‖‡
Epi	−9.5 ± 0.4	−1.8 ± 0.6*	−1.1 ± 1.0*	2.5 ± 0.6*‖‡
E_2				
Endo	−16.5 ± 0.4	−8.4 ± 0.4*	−11.8 ± 0.9*	−8.6 ± 0.5*‡
Mid	−13.7 ± 0.3	−8.2 ± 0.5*	−10.3 ± 0.7†	−7.5 ± 0.4*‡
Epi	−13.2 ± 0.4	−8.7 ± 0.7*	−11.2 ± 0.9†	−8.0 ± 0.5*‡
E_2 direction				
Endo	16.0 ± 0.8	36.2 ± 2.7*	45.1 ± 3.3*	52.9 ± 2.7*‖§
Mid	17.2 ± 0.8	40.5 ± 2.8*	47.1 ± 3.3*	57.6 ± 1.8*‖‡
Epi	23.0 ± 1.0	44.8 ± 2.8*	49.4 ± 2.9*	59.1 ± 1.7*‖‡
Err				
Endo	18.1 ± 1.3	4.0 ± 1.8*	2.4 ± 1.7*	0.0 ± 0.9*‖§
Mid	15.6 ± 1.6	1.4 ± 1.8*	2.2 ± 1.9*	−1.4 ± 0.9*§
Epi	10.2 ± 1.4	−0.6 ± 1.3*	−0.5 ± 1.9*	−1.8 ± 1.0*§
E_1				
Endo	26.9 ± 1.8	15.8 ± 1.9*	22.3 ± 3.2†	21.1 ± 1.5†
Mid	23.0 ± 1.6	12.6 ± 1.4*	18.6 ± 2.4†	15.8 ± 1.0†
Epi	18.6 ± 1.3	11.8 ± 1.4†	17.2 ± 1.8	14.0 ± 1.0†

*$p < 0.0001$; †$p < 0.05$ vs. remote; ‡$p < 0.01$; §$p < 0.05$ vs. TTC < 1/3 wall; ‖$p < 0.05$ vs. risk. E_2 direction is the angle between the direction of Ecc and that of E_2.

E_{cc} = circumferential; endo = endocardium; epi = epicardium; Err = radial; E_1 = maximal thickening; E_2 = maximal shortening; mid = midwall.

Moreover, E_2 direction shifted significantly from the circumferential direction ($p < 0.0001$ for both risk and infarcted vs. remote regions). Slight, but significant, differences in myocardial strains were found between risk and infarcted segments. Stretching in the circumferential direction was observed in transmurally infarcted segments as opposed to shortening in risk regions ($p < 0.05$). Similarly, E_2 direction shifted further away from the circumferential direction, and radial thickening in the subendocardial layer was lower in transmurally infarcted versus risk regions ($p < 0.05$) (Table 2).

Strains and infarct transmural extent. Among infarcted segments, 61 showed infarct limited to the subendocardium (subendocardial infarcts one-third of wall thickness), and 129 exhibited transmural infarct extent >one-third of the LV wall thickness (that is, transmural infarcts). Circumferential shortening and E_2 were reduced uniformly across the wall in both transmural and subendocardial infarcts ($p < 0.01$, from subendocardium to subepicardium for both) (Table 2). Maximal shortening angle from the circumferential direction was higher in transmural versus nontransmural infarcts ($p < 0.05$ for subendocardium and $p < 0.01$ for midwall and subepicardium). Radial thickening was greater in segments with subendocardial as compared with segments with transmural infarcts ($p < 0.05$).

Recruitable myocardial strains under dobutamine. Circumferential shortening and E_2 were greater during stress versus rest in remote, risk and infarcted regions (Fig. 2). However, the stress-induced increase in myocardial shortening measured in infarcted segments was entirely caused by a significant shortening increase in regions with subendocardial infarct by TTC (−4.5 ± 1.2 vs. −1.5 ± 1.1% for E_{cc} and −12.5 ± 1.0 vs. −11.1 ± 0.8% for E_2, both $p < 0.01$). This local increase in function resulted from a uniform transmural augmentation of myocardial strains (−6.3 ± 1.4 vs. −2.0 ± 1.4% in subendocardium, −4.1 ± 1.3 vs. −1.4 ± 1.1% in midwall, −3.1 ± 1.1 vs. −1.1 ± 1.0% in subepicardium for Ecc, $p < 0.01$; −12.9 ± 1.4 vs. −11.8 ± 0.9%, −11.9 ± 1.1 vs. −10.3 ± 0.7% and −12.7 ± 0.8 vs. −11.2 ± 0.9% for E_2, respectively, $p < 0.01$) (Fig. 3). Conversely, myocardial shortening was not significantly higher during stress in segments with transmural infarct (2.0 ± 0.9 vs. 2.7 ± 0.7% and −8.9 ± 0.7 vs. −8.0 ± 0.5% for Ecc and E_2, respectively, $p =$ NS) (Fig. 4). Finally, the direction of maximal shortening (E_2) shifted slightly away from the circumferential direction under dobutamine versus rest in remote regions. Conversely, under dobutamine stimulation, E_2 direction was more circumferentially oriented in risk and infarcted regions as compared with rest regions ($p < 0.01$) (Fig. 2).

Dobutamine infusion was also responsible for an increase in Err and E_1 in remote, risk and infarcted regions ($p < 0.01$) (Fig. 2). However, similar to shortening, inotropic stimulation led to a significant increase in Err and E_1 in segments with subendocardial infarcts by TTC (3.0 ± 1.4 vs. 1.0 ± 1.8% and 22.9 ± 2.7 vs. 19.4 ± 2.4%, respectively, $p < 0.01$) but not in regions with transmural infarction (0.0 ± 1.6 vs. −1.0 ± 0.9% and 17.7 ± 1.6 vs. 17.0 ± 1.2%, respectively, $p =$ NS). In addition, the stress-induced augmentation of wall thickening in segments with suben-

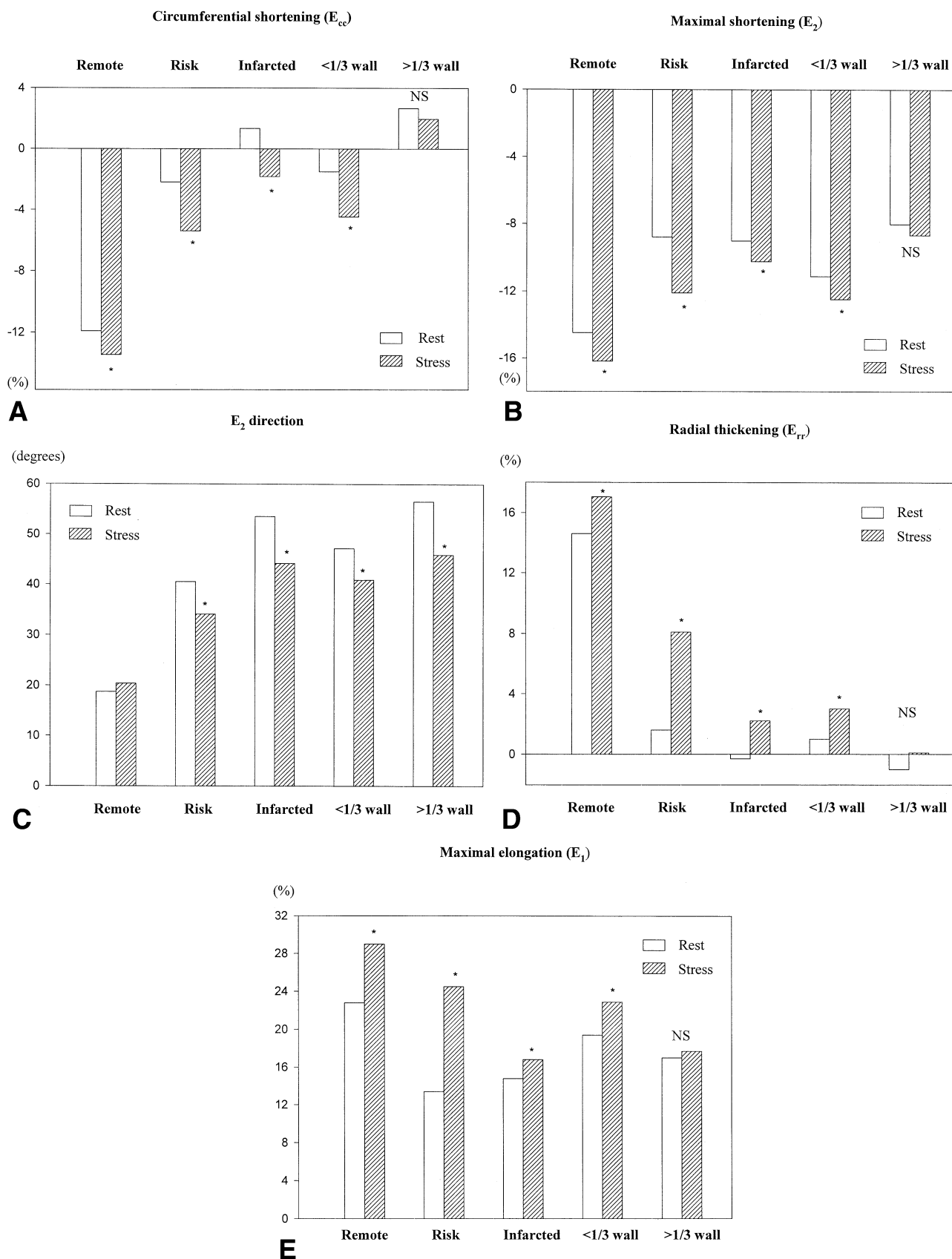**Figure 2.** Circumferential shortening (E_{cc}) (**A**), maximal shortening (E_2) (**B**), E_2 direction (**C**), radial thickening (Err) (**D**) and maximal elongation (E_1) (**E**) are shown in remote, risk and infarcted myocardium at rest and 5 $\mu g \cdot kg^{-1} \cdot min^{-1}$ dobutamine. Infarcted = combination of segments with infarct extension $\geq 1/3$ of wall thickness. *p < 0.01 versus rest.
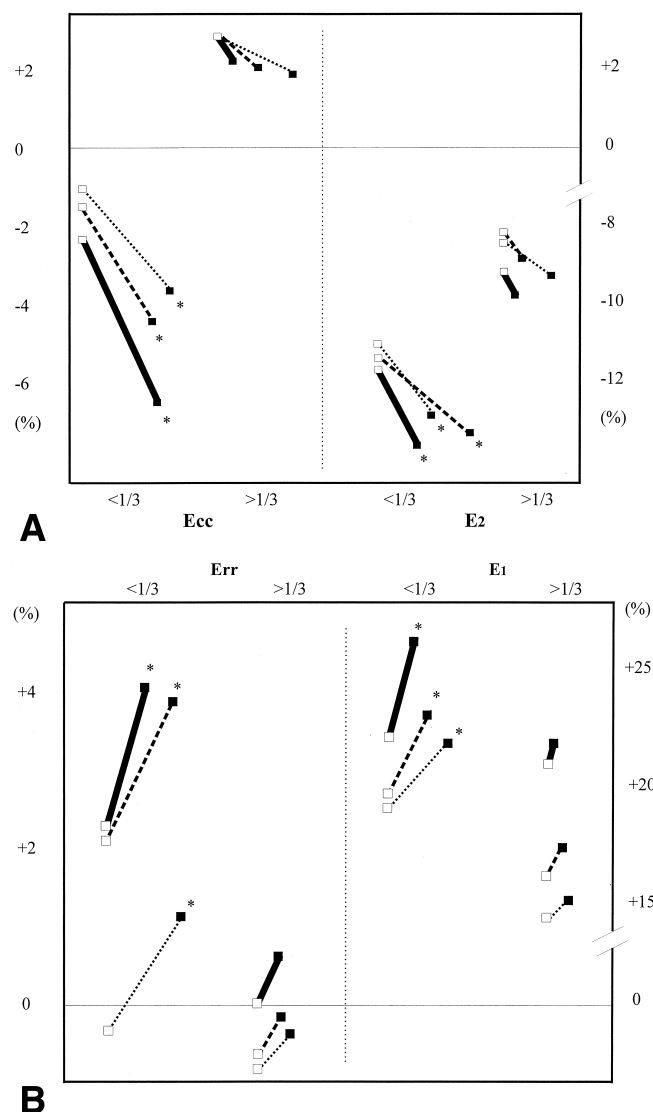
Figure 3. Transmural contractile reserve as assessed for circumferential shortening (Ecc) and maximal shortening (E_2). (**A**) Radial thickening (Err) and maximal elongation (E_1). (**B**) In segments with subendocardial ($\leq 1/3$) and transmural extent ($> 1/3$ of wall thickness) of infarct. **open squares** = rest; **closed squares** = dobutamine; **black line** = subendocardium; **large dotted line** = midwall; **small dotted line** = subepicardium. *p < 0.01 versus rest.

docardial infarction was due to a homogeneous increase in strains across the LV wall (4.0 ± 1.6 vs. 2.4 ± 1.7% in subendocardium, 3.8 ± 1.6 vs. 2.2 ± 1.9% in midwall and 1.2 ± 1.1 vs. −0.5 ± 1.9% in subepicardium for Err, p < 0.01; 25.4 ± 3.2 vs. 22.3 ± 3.2%, 22.6 ± 2.9 vs. 18.6 ± 2.4% and 20.7 ± 1.9 vs. 17.2 ± 1.8% for E_1, respectively, p < 0.01) (Fig. 3).

DISCUSSION

This is the first study to analyze in detail transmural functional reserve within different regions of the infarcted LV. We used HARP from tagged-MRI to measure various myocardial strains transmurally, at rest and under inotropic stimulation, in a model of reperfused canine infarction with

histopathologic specimens and MBF as gold standards. As opposed to transmural infarcts, which exhibit systolic stretching in the circumferential direction and no wall thickening (or wall thinning), myocardial shortening and thickening were observed at rest in the outer and inner layers of segments with subendocardial infarcts. In these segments passive deformation at rest in inner layers is indistinguishable from outer layers' active deformation. More importantly, it increases under dobutamine due to the recruitment of function in the outer subepicardial layers. These findings support the concept that the recruitment of myofiber shortening and cross-fiber shortening in midlayers and outer layers of the myocardial wall lead to passive thickening in the infarcted subendocardium. Additionally, the quantitative analysis of myocardial strains by HARP was able to depict transmural differences in local inotropic reserve within reperfused-viable and reperfused-infarcted myocardium.

Relation of histopathology and myocardial perfusion to myocardial strains within postischemic injured myocardium. *Strains in risk versus infarcted regions.* Little is known about the differences in segmental contractile performance as assessed at rest in reversibly versus irreversibly damaged myocardium. We show that normal strains (Ecc, Err) at rest were greater in risk regions versus infarcted regions. Whereas the magnitude of principal strains remained unchanged, the direction of the minimal principal strain (E_2) shifted further away from the circumferential direction in infarcted versus risk regions. Previous studies have shown that systolic myocardial deformation is reduced in the adjacent segments to infarcted myocardium (18) and further reduced in tissue perfused by mixed ischemic and nonischemic blood supply (19). In addition, the central core of the infarct often remains nonreperfused after the release of prolonged coronary occlusion (20). This no-reflow phenomenon represents a strong predictor of further LV remodeling (21), possibly through local changes in mechanical properties of the myocardium (7). Our findings support the concept that alterations of regional function within the infarcted region are not homogeneous, with gradual increase in strains from the center to the surrounding area of the ischemic territory.

Infarct transmural extent and myocardial strains. Radial thickening, Ecc and E_2 were clearly decreased in transmural, as compared with subendocardial infarcts. Greater subendocardial shortening and thickening in segments with subendocardial versus transmural infarcts were unexpected. When isolated fibers shorten, they thicken in the two orthogonal directions (8). The nonparallel myocardial fiber orientation within the LV wall (5) permits the interaction of fibers at different depths within the wall. This results in a structural rearrangement that enables shortening to occur not only along the fibers long-axis but also perpendicular to it (6). Such "cross-fiber shortening," which predominates in the inner layers of the LV wall, enables relatively small amounts of myofiber shortening to cause extensive wall
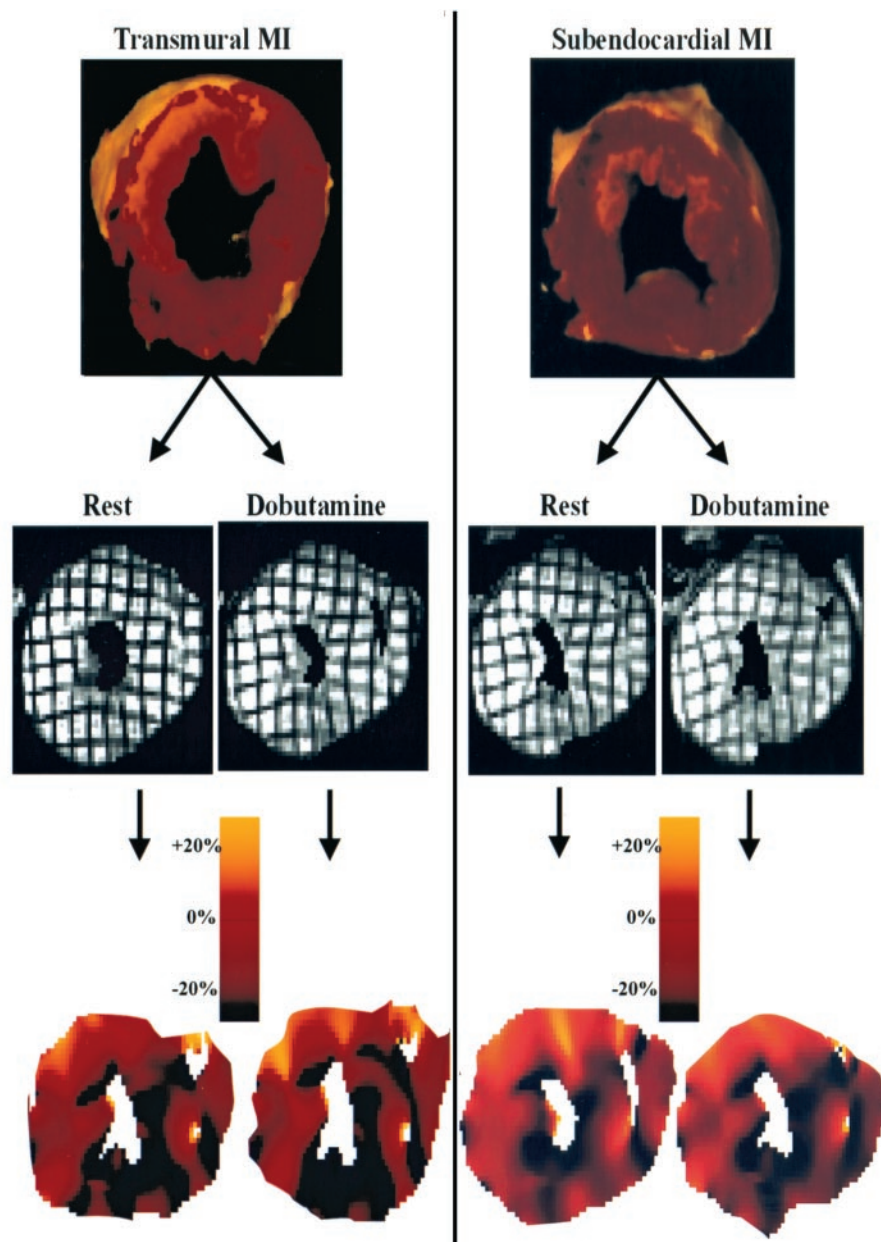
Figure 4. Histopathologic specimens of the left ventricular myocardium (**upper panel**) in dogs with transmural (**left**) and subendocardial (**right**) reperfused anterior infarct. The corresponding short-axis tagged images of the left ventricle at end-systole, at rest and 5 $\mu g \cdot kg^{-1} \cdot min^{-1}$ dobutamine are shown in **midpanel**. Regional myocardial strain maps (circumferential shortening) by harmonic phase imaging are displayed in the **lower panel**. **Black** indicates shortening and **yellow** indicates stretching. MI = myocardial infarction.

thickening (6). Our data show that cross-sectional shape changes of myofibers in midlayers and outer layers of the LV wall contribute to the "passive wall thickening" observed during contraction in the inner layers of segments with subendocardial infarction. Prior studies have reported significant "passive systolic wall thickening" three weeks after infarction in regions composed almost entirely of collagen (7). Since no active shortening occurs in the inner layers of segments with subendocardial infarcts, the small, but significant, amount of fiber shortening observed in those layers is likely to result from interaction with differently aligned fibers located at a distance (8). Indeed, previous studies have shown that cross-fiber shortening in the outer layers is

closely related to endocardial fiber shortening in the normal human heart, stressing the strong interaction that exists between different layers of the myocardium (8).

Recruitment of LV function and implications to myocardial viability assessment. In agreement with other previous studies (22), we found regional contractile reserve to be at greater risk than infarcted regions. Those segments most likely contain stunned myocardium caused by a single, completely reversible episode of regional ischemia (23). Interestingly, normal (Ecc, Err) and principal strains (E_2, E_1) augmented under inotropic stimulation in segments with subendocardial infarcts that also had a homogeneous transmural strain increase. The implications with regard to

our results for the clinical assessment of myocardial viability for patients with acute MI are obvious. The detection of recruitable regional wall thickening or shortening in the inner half of the myocardial wall does not imply that the inner layers are not infarcted. These findings demonstrate that the recruitment of regional function in midlayers and outer layers of the LV wall may play an important role in the subsequent recovery of segmental cardiac function. Geskin et al. (2), using MR tissue tagging, have demonstrated that the local contractile response to dobutamine after MI is predictive of subsequent recovery of LV function. However, the response in midwall and subepicardium was predictive, whereas that in the subendocardium was not. Our study demonstrates that recruitable myocardial deformation can be detected in the subendocardium of segments with subendocardial infarcts. Since the subendocardium plays an important role in regional LV function at rest, those segments may still have subsequent impaired function when assessed at rest during follow-up, accounting for the mismatch between their apparent contractile response to dobutamine and the absence of subsequent recovery. These data provide new insights into the transmural distribution of the dobutamine-induced recruitment of local myocardial function within postischemic injured myocardium.

We measured two-dimensional myocardial strain fields and did not compensate for through-plane translation of the heart (24). However, two-dimensional myocardial strains determined from tissue tagging are sufficiently powerful to accurately index myocardial ischemia (25). Although still in development, measurements of myocardial deformation by HARP are extendable to three-dimensional analysis (12,13).

Conclusions. Tagged-MR cardiac images analyzed by the HARP method allow for rapid and detailed transmural assessment of local contractile reserve after acute MI. Risk regions retained maximal contractile reserve, and no functional reserve was found in segments with transmural infarction. However, under dobutamine stimulation, myofiber shortening increase in midlayers and outer layers of segments with subendocardial infarcts led to significant augmentation of passive thickening and shortening in the subendocardium. These results may have important implications in the clinical detection of myocardial viability in humans.

REFERENCES

1. Marwick TH. The viable myocardium: epidemiology, detection and clinical implications. Lancet 1998;351:815–9.
2. Geskin G, Kramer CM, Rogers WJ, et al. Quantitative assessment of myocardial viability after infarction by dobutamine magnetic resonance tagging. Circulation 1998;98:217–23.
3. Baer FM, Theissen P, Schneider CA, et al. Dobutamine magnetic resonance imaging predicts contractile recovery of chronically dysfunctional myocardium after successful revascularization. J Am Coll Cardiol 1998;31:1040–8.
4. Picano E, Lattanzi F, Orlandini A, Marini C, L'Abbate A. Stress echocardiography and the human factor: importance of being expert. J Am Coll Cardiol 1991;17:666–9.
5. Streeter DD Jr, Spotnitz HM, Patel DP, Ross J Jr, Sonnenblick EH. Fiber orientation in the canine left ventricle during diastole and systole. Circ Res 1969;24:339–47.
6. Waldman LK, Nosan D, Villarreal F, Covell JW. Relation between transmural deformation and local myofiber direction in canine left ventricle. Circ Res 1988;63:550–62.
7. Holmes JW, Yamashita H, Waldman LK, Covell JW. Scar remodeling and transmural deformation after infarction in the pig. Circulation 1994;90:411–20.
8. Rademakers FE, Rogers WJ, Guier WH, et al. Relation of regional cross-fiber shortening to wall thickening in the intact heart: three-dimensional strain analysis by NMR tagging. Circulation 1994;89:1174–82.
9. Zerhouni EA, Parish DM, Rogers WJ, Yang A, Shapiro EP. Human heart: tagging with MR imaging: a method for noninvasive assessment of myocardial motion. Radiology 1988;169:59–63.
10. Axel L, Dougherty L. Magnetic resonance imaging of motion with spatial modulation of magnetization. Radiology 1989;171:841–5.
11. O'Dell WG, Moore CC, Hunter WC, Zerhouni EA, McVeigh ER. Three-dimensional myocardial deformations calculation with displacement field fitting to tagged MR images. Radiology 1995;195:829–35.
12. Osman NF, Prince JL. Angle images for measuring heart motion from tagged MRI. Proceedings of IEEE Conference on Image Procedures. Chicago:1998:I704–8.
13. Osman NF, Faranesh AZ, McVeigh ER, Prince JL. Tracking cardiac motion using cine harmonic phase (HARP) magnetic resonance imaging. Proceedings of the ISMRM. Philadelphia:1999:22–8.
14. Garot J, Bluemke DA, Osman NF, et al. Fast determination of regional myocardial strain fields from tagged cardiac images using harmonic phase (HARP) magnetic resonance imaging. Circulation 2000;101:981–8.
15. McVeigh ER, Atalar E. Cardiac tagging with breath-hold cine MRI. Magn Reson Med 1992;28:318–27.
16. Fishbein MC, Meerbaum S, Rit J, et al. Early phase acute myocardial infarct size quantification: validation of the triphenyl tetrazolium chloride tissue enzyme staining technique. Am Heart J 1981;101:593–600.
17. Ambrosio G, Weisman HF, Mannisi JA, Becker LC. Progressive impairment of regional myocardial perfusion after initial restoration of postischemic blood flow. Circulation 1989;80:1846–61.
18. Lima JAC, Becker LC, Melin JA, et al. Impaired thickening of nonischemic myocardium during acute regional ischemia in the dog. Circulation 1985;71:1048–59.
19. Gallagher KP, Gerren RA, Stirling MC, et al. The distribution of functional impairment across the lateral border of acutely ischemic myocardium. Circ Res 1986;58:570–83.
20. Kloner RA, Ganote CE, Jennings RB. The "no-reflow" phenomenon after temporary coronary occlusion in the dog. J Clin Invest 1974;54:1496–508.
21. Wu KC, Zerhouni EA, Judd RM, et al. The prognostic significance of microvascular obstruction by magnetic resonance imaging in patients with acute myocardial infarction. Circulation 1998;97:765–72.
22. Croisille P, Moore CC, Judd RM, et al. Differentiation of viable and nonviable myocardium by the use of three-dimensional tagged MRI in 2-day-old reperfused canine infarcts. Circulation 1999;99:284–91.
23. Bolli R, Marban E. Molecular and cellular mechanisms of myocardial stunning. Physiol Rev 1999;79:609–34.
24. Rogers WJ, Jr, Shapiro EP, Weiss JL, et al. Quantification of and correction for left ventricular systolic long-axis shortening by magnetic resonance tissue tagging and slice isolation. Circulation 1991;84:721–31.
25. Lima JAC, Jeremy R, Guier W, et al. Accurate systolic wall thickening by nuclear magnetic resonance imaging with tissue tagging: correlation with sonomicrometers in normal and ischemic myocardium. J Am Coll Cardiol 1993;21:1741–51.